Title
Calvarial Defect Healing Induced by Small Molecule Smoothened Agonist.

Journal
Tissue engineering. Part A, 22(23-24)

ISSN
1937-3341

Authors
Lee, Soonchul
Shen, Jia
Pan, Hsin Chuan
et al.

Publication Date
2016-12-01

DOI
10.1089/ten.tea.2016.0167

Peer reviewed

TISSUE ENGINEERING: Part A
Volume 22, Numbers 23 and 24, 2016

DOI: 10.1089/ten.tea.2016.0167

termis
Tissue Engineering
& Regenerative Medicine
International Society

ORIGINAL ARTICLE

Calvarial Defect Healing Induced by Small Molecule Smoothened Agonist

Soonchul Lee, MD, PhD,[1–3,*] Jia Shen, PhD,[1,*] Hsin Chuan Pan, DDS,[1] Swati Shrestha, BS,[3] Greg Asatrian, BS,[1] Alan Nguyen, BS,[1] Carolyn Meyers, BS,[4] Vi Nguyen, BS,[1] Min Lee, PhD,[5] Chia Soo, MD, FACS,[3,6] Kang Ting, DMD, DMedSci,[2,3] and Aaron W. James, MD, PhD[3,4]

Hedgehog (Hh) signaling positively regulates both endochondral and intramembranous ossification. Use of small molecules for tissue engineering applications poses several advantages. In this study, we examined whether use of an acellular scaffold treated with the small molecule Smoothened agonist (SAG) could aid in critical-size mouse calvarial defect repair. First, we verified the pro-osteogenic effect of SAG *in vitro*, using primary neonatal mouse calvarial cells (NMCCs). Next, a 4 mm nonhealing defect was created in the mid-parietal bone of 10-week-old CD-1 mice. The scaffold consisted of a custom-fabricated poly(lactic-co-glycolic acid) disc with hydroxyapatite coating (measuring 4 mm diameter × 0.5 mm thickness). Treatment groups included dimethylsulfoxide control ($n=6$), 0.5 mM SAG ($n=7$) or 1.0 mM SAG ($n=7$). Evaluation was performed at 4 and 8 weeks postoperative, by a combination of high-resolution microcomputed tomography, histology (H & E, Masson's Trichrome), histomorphometry, and immunohistochemistry (BSP, OCN, VEGF). *In vivo* results showed that SAG treatment induced a significant and dose-dependent increase in calvarial bone healing by all radiographic parameters. Histomorphometric analysis showed an increase in all parameters of bone formation with SAG treatment, but also an increase in blood vessel number and density. In summary, SAG is a pro-osteogenic, provasculogenic stimulus when applied locally in a bone defect environment.

Keywords: osteogenesis, vasculogenesis, bone healing, small molecule, smoothened agonist, hedgehog signaling

Introduction

Skeletal nonunion is a postoperative risk associated with all surgical bone fracture repairs, often requiring costly long-term therapy. Despite the regenerative and reparative capacity of bone, approximately 5% to 10% of fractures are associated with impaired healing.[1] Consequently, nonhealing skeletal defects are addressed in over 2.2 million bone graft surgeries each year worldwide.[2] Autologous bone graft from the iliac crest is considered the preferred method for nonhealing bone defect repair.[3,4] However, autologous bone graft is limited in supply and requires an additional surgical incision, which can be associated with increased pain, neurologic injury, infection, and hematoma.[5,6] Thus, various osteoinductive growth and differentiation factor (GDF)-based therapies have been developed in an attempt to induce bone healing and eliminate the need for autologous bone grafts.

Recombinant human bone morphogenetic protein-2 (rhBMP-2, INFUSE®; Medtronic Sofamor Danek) is the most commonly used osteogenic factor for orthopedic applications within the United States, approved by the Food and Drug Administration for lumbar interbody fusion and tibial nonunion. Nevertheless, it possesses several side effects,

[1]Division of Growth and Development and Section of Orthodontics, School of Dentistry, University of California, Los Angeles, Los Angeles, California.
[2]Department of Orthopaedic Surgery, CHA Bundang Medical Center, CHA University, Republic of Korea.
[3]Department of Orthopaedic Surgery and the Orthopaedic Hospital Research Center, University of California, Los Angeles, Los Angeles, California.
[4]Department of Pathology, Johns Hopkins University, Baltimore, Maryland.
[5]Section of Biomaterials, School of Dentistry, University of California, Los Angeles, Los Angeles, California.
[6]Division of Plastic and Reconstructive Surgery, Department of Surgery, David Geffen School of Medicine, University of California, Los Angeles, Los Angeles, California.
*These authors contributed equally to this work.

including life-threatening inflammatory swelling, promotion of adipogenesis and cystic bone formation, as well as activation of osteoclast activity.[7,8] With this potentially worrisome side effect profile, the search for novel osteoinductive alternatives to rhBMP-2 is imperative.

The Hedgehog (Hh) signaling family includes three mammalian ligands, Sonic hedgehog (Shh), Indian hedgehog (Ihh), and Desert hedgehog (Dhh), all have well-described importance in diverse developmental processes.[9] The activity of the Hh pathway was first identified in Drosophila, and its expression was later found in all vertebrates. All of the Hh homologues undergo the same highly conserved Hh signaling pathway.[10] First, the insoluble Hh morphogen is converted to a multimeric form, which renders it soluble and available for diffusion across cell membranes. Second, a large transmembrane protein, Dispatched, releases the now lipid-anchored protein Hh from the signaling cell, which allows Hh binding to the receptor Patched (Ptc), a transcription inhibitor. After the Hh ligand binds to Ptc, Smoothened (Smo), another transmembrane protein for downstream signaling, is freed from Ptc repression and transduces the signal intracellularly. In vertebrates, Smo leads to the transcription of target genes downstream through interaction with glioblastoma gene products (Gli) family of transcription factors (Gli1, Gli2, and Gli3). Recently, the so-called ''noncanonical Hh signaling pathway'' has been discovered, which utilizes Gli-independent pathways.[11]

Hh signaling is well known to stimulate differentiation of osteoprogenitor cells and mesenchymal stem/stromal cells (MSC), as observed using both osteoblastic cell lines and primary cell cultures.[12–19] While the exact mechanism and stage at which Hh acts during osteoblastogenesis are not completely understood, both *in vivo* and *in vitro* data suggest that bone formation occurs through a positive feedback loop. Hh-induced osteoblastogenesis appears to require BMP signaling, and together they elicit a synergistic expression of alkaline phosphatase activity.[12] This positive feedback loop is further mediated by Gli2 transcription, which serves to upregulate BMP-2 expression, which in turn activates Gli transcription.[16] In the murine MSC line C3H10T1/2, Hh simultaneously induced osteoblastic differentiation.[13–15] In KS483 cells, a similar induction of osteogenesis by Shh was reported.[19] It is important to note that Shh-induced differentiation was only observed in immature mesenchymal cell lines 3H10T1/2 and not preosteoblastic MC3T3-E1 or osteoblastic cell lines OS 17/2.8 and ROB-C26.[12,15] Later studies observed that Shh induces osteogenic differentiation of adipose-derived stromal cells from either mouse or human origin.[17,18] Collectively, these data imply that the Hh activity and Shh may be key in stimulating osteoblastogenesis, primarily during early stages of osteodifferentiation.

High-throughput screening of chemical libraries has identified the Smo agonist (SAG) as the activator of intracellular Hh signaling.[20–22] SAG was discovered in Shh-LIGHT2 cells and consists of a chlorobenzothiophene-containing small molecule.[21] SAG facilitates the translocation of the Smo from cytoplasm to primary cilium and stabilizes it in its active form.[23] More recently, it was reported that SAG promotes osteoblast differentiation in osteochondrogenitor cells within the perichondrium.[24] Also, pluripotent stem cells have been reported to successfully differentiate into osteoblasts using various small molecules, including SAG.[25]

Despite the well-known osteoinductive effects of Hh signaling, only limited information is available regarding the *in vivo* use of SAG. In this study, for the first time, we examined the osteoinductive effects of the small molecule SAG in a nonhealing bone defect model.

Materials and Methods

Cell culture

Neonatal mouse calvarial cells (NMCCs) were obtained from newborn mouse calvaria as previously described.[26] Cells were expanded in the α-minimum essential medium (α-MEM) supplemented with 10% fetal bovine serum (Life Technologies, Inc.), 100 U/mL of penicillin, and 100 μg/mL of streptomycin. For all assays, passage 2–3 cells only were used. Cells were seeded onto six-well plates at a density of 100,000 cells/well. The osteogenic differentiation medium included the addition of 100 μg/mL of l-ascorbic acid and 10 mM glycerophosphate supplemented with or without SAG (0.5 or 1.0 μM) or dimethylsulfoxide (DMSO) control (0.1% solution). At 0, 7, 14, and 21 days after differentiation, gene expression among NMCCs was examined.

RNA isolation and quantitative real-time polymerase chain reaction

Total RNA was isolated from cells and tissue as previously described.[17,27–30] For cells, after two washes in cold sterile PBS, cells were lysed with a cell scraper, followed by isolation with the RNeasy Mini Kit (Qiagen Sciences). Reverse transcription was performed with 1 μg RNA using TaqMan Reverse Transcription Reagents (Applied Biosystems). Quantitative real-time polymerase chain reaction (qRT-PCR) was carried out using the Applied Biosystems Prism 7900HT Sequence Detection System and Sybr Green PCR Master Mix (Applied Biosystems). Specific primers for the genes examined were based on their PrimerBank sequence and are listed in Supplementary Table S1 (Supplementary Data are available online at www.liebertpub.com/tea).

Animals and preparation of scaffold

Ten-week-old twenty CD-1 male mice weighing approximately 25–29 g were obtained from Charles River Laboratories and were used for the experiment. Each was housed in a single pathogen-free ventilated cage, fed a standard rodent chow diet, and provided tap water *ad libitum*. All mice were handled according to the guidelines of the Chancellor's Animal Research Committee for Protection of Research Subjects at the University of California, Los Angeles.

Hydroxyapatite-coated poly(lactic-co-glycolic acid) (PLGA) was used as the scaffold for SAG delivery. PLGA scaffolds fabrication was performed as previously described.[31] Custom-fabricated scaffold dimensions were 4 mm in diameter and 0.5 mm in thickness. Next, a simulated body fluid solution was used for apatite coating of the surface of the scaffolds, as previously described.[32,33] After apatite coating, scaffolds were disinfected by immersion in 70% ethanol, followed by three rinses in ddH_2O. All scaffolds were then dried under a laminar flow hood. Next, three treatment groups of apatite-coated scaffolds were prepared 24 h before surgery by adsorbing with

(1) DMSO as a control, (2) SAG (0.5 mM), and (3) SAG (1.0 mM). SAG was purchased from EMD Millipore Co.

Surgical procedure

Nonhealing, critical-sized (4 mm) calvarial defects were created in the right parietal bone of mice. After anesthesia with an isoflurane and oxygen mixture, a subcutaneous injection of buprenorphine (0.05 mg/kg) was given for analgesia, the hair over the skull was shaved, and the underlying skin was aseptically prepared using proviodine/betadine scrub. Subsequently, the animal was transferred onto a heating pad (maintained at 37°C) in the operating field. A sagittal skin incision was made over the scalp from the nasal bone to the middle sagittal crest and the pericranium was removed from the right parietal bone. A unilateral 4 mm full-thickness defect was created using a dental surgical drilling unit with a trephine. Sutures were excluded, leaving the dura mater undisturbed. Before scaffold placement, calvarial defect sites were copiously irrigated by saline to wash out any bone fragments (Supplementary Fig. S1). Animals were divided into three treatment groups: (1) Control group: 0.01% DMSO on scaffold, in which a PLGA scaffold without SAG was placed in the defect site ($n=6$), (2) 0.5 mM SAG group: SAG on a scaffold, in which 0.5 mM SAG was impregnated in a scaffold and this was then placed in the defect site ($n=7$), and (3) 1.0 mM SAG group: 1.0 mM SAG on a scaffold ($n=7$). Finally, the skin was sutured and the animal was monitored per established postoperative protocols.

In vivo *live microcomputed tomography imaging and analyses*

At 4 and 8 weeks after surgery, the healing of the defect site was evaluated. Live imaging was performed using a high-resolution microcomputed tomography (micro-CT) (SkyScan 1176; Bruker MicroCT N.V.) at an image resolution of 18 μm, with the following settings: 0.5 mm of aluminum filter, X-ray voltage of 50 kVp, anode current of 500 mA, exposure time of 250 ms, frame averaging of 2, and rotation step of 0.4 degrees. After imaging, animals were allowed to recover before being returned to the animal facility.

Three dimensional images were then reconstructed from the 2D X-ray projections by implementing the Feldkamp algorithm. Appropriate image corrections were made, including ring artifact correction, beam hardening correction, and fine-tuning using NRecon software (1.6.10.4 SkyScan). For the 3D morphometric analyses of images, CT-Analyzer software (1.16.1.0 SkyScan) was used. The cylindrical volume of interest was defined as the 4 mm in diameter and the 1 mm in height to include all the new bone formation in the calvarial defect site.

The amount of bone formation was analyzed and quantified in three different ways by comparing scans to those on the same animal taken postoperatively. First, parameters, including bone volume density (bone volume/tissue volume, BV/TV [%]) and bone mineral density (BMD, g/cm^3), were calculated from the binary images. Second, analyses of bone fractional area (BFA [%]) were performed to determine the area within the defect covered by new bone formation. After the 3D volume of interest was reprojected onto a 2D plane using the maximum intensity projection tool of ImageJ software (National Institutes of Health), 4 mm diameter of region of interest was then centered on the calvarial defect.[34] Third, after 3D rendered models were generated for the visualization of analyzed regions using the marching cubes method, the extent of bone formation within the calvarial defect was scored. A bone healing score from 0 to 4 was assigned by a blinded observer according to previous published grading scales for calvarial defect healing.[35] Briefly the grading was as follows: 0–no bone formation, 1–few bony spicules dispersed through defect, 2–bony bridging only at defect borders, 3–bony bridging over partial length of defect, and 4–bony bridging entire span of defect at longest point.

Harvest and histologic analysis

Eight weeks postoperatively, animals were sacrificed for histology. After anesthesia with 4.5% isoflurane/oxygen, the gas was switched to carbon dioxide for asphyxiation followed by a bilateral thoracotomy as a secondary method of euthanasia. Calvaria were harvested, formalin fixed, decalcified in 19% EDTA, paraffin imbedded, and sectioned at 5 μm thickness.

Using the decalcified samples, hematoxylin and eosin (H & E) and Masson's Trichrome staining were performed on deparaffinized sections as previously described.[36] Then, under light microscopy, images of stained cross-sections of each sample at the level of the calvarial defect were obtained from each mouse and analyzed histomorphometrically using Photoshop software, including the following parameters: (1) Bone Area (B.Ar): number of pixel per high power field (HPF), (2) Fractional Bone Area (B.Ar/T.Ar): bone as a fraction of tissue Area (T.Ar), (3) Blood Vessel Area (BV.Ar), and (4) Blood Vessel Number (BV.N): whole number integer per HPF. Analyses performed on images obtained from 6 to 12 adjacent HPF so as to encompass the entire defect site of each animal on a representative mid-defect section.

For immunohistochemistry, additional sections were incubated with the following primary antibodies: anti-osteocalcin (OCN) (1/100; Santa Cruz Biotechnology), anti-bone sialoprotein (BSP) (1/2500; Millipore), and anti-VEGF (sc-7269; Santa Cruz Biotechnology, 1/100). The following secondary antibodies were used: biotinylated anti-rabbit or anti-goat IgG secondary antibody (1/200; Dako). The paraffin slices were deparaffinized, dehydrated, rinsed, and incubated with 3% H_2O_2 for 20 min using the ABC (Vector Laboratories, Inc.) method. Trypsin-induced epitope retrieval was performed for 20 min at room temperature, using the ''Digest-All 2'' system (Cat 00-3008; Invitrogen). All sections were then blocked with 0.1% bovine serum albumin in PBS for 1 h. Primary antibodies were added to each section at their respective dilutions and incubated at 37°C for 1 h or overnight at 4°C. Positive immunoreactivity was detected following ABC complex (PK-6100, Vectastain Elite ABC Kit; Vector Laboratories, Inc.) incubation and development with AEC chromagen (K346911-2; Dako). Mayer's hematoxylin (1/5; Abcam) was used as a nuclear counterstain and slides were mounted using an aqueous media (VectaMount AQ, Vector Laboratories).

Statistical analysis

Means and standard deviations were calculated from numerical data, as presented in the text, figures, and figure

legends. In figures, bar graphs represent means, whereas error bars represent one standard deviation. The means of groups were compared using the Mann–Whitney U test when only two data sets were being compared and by the Kruskal–Wallis test with *post hoc* tests of Bonferroni to compare more than two groups. In addition, because three independent observers scored the defect site, intraclass correlation coefficient was analyzed. The statistical software SPSS for Windows Version 18.0 (SPSS) was used for all statistical analyses. Statistical significance was determined at the $p < 0.05$ level.

Results

SAG increased osteogenic differentiation in mouse NMCCs

First, to verify the pro-osteogenic effect of SAG *in vitro*, treatment of NMCCs with SAG (0.5 or 1.0 μM) was performed and gene markers associated with osteogenesis were assessed by qRT-PCR (Fig. 1). Markers assessed included *Osteocalcin (Ocn), Osteopontin (Opn), Osteonectin (On), Bone Sialoprotein (Bsp),* and *Type 1 Collagen (Col 1)*. Presented results are normalized to day 0 expression levels (immediately before differentiation). Results showed under control conditions (white bars), all markers increased in transcript abundance overtime under osteogenic differentiation conditions until 21 days. Also, expression of all osteogenic markers was increased with SAG treatment among NMCCs, with differences achieving statistical significance among most specific genes and time points examined ($*p < 0.05$, $**p < 0.01$).

SAG augments critical-size mouse calvarial bone healing

Radiographic evaluation of bone regeneration. To test the *in vivo* bone induction by SAG, a 4 mm parietal bone defect model in the mouse was used (Supplementary Fig. S1). To evaluate the progressive bone defect healing, *in vivo* micro-CT imaging was examined at 4 and 8 weeks postoperative. Images are shown as either whole skull reconstructions (Fig. 2A) or time lapse micro-CT images of the defect site (Fig. 2B), in which progressive defect reossification can be appreciated by colorized reconstructions at 4 and 8 weeks overlaid on one another. In general, SAG treatment resulted in a dose-dependent increase in defect reossification, with the most prominent bone formation occurring with the 1.0 mM treatment group. As expected from a nonhealing defect type, there was little evidence of defect reossification with the control-treated scaffold.

Next, a previously characterized qualitative scale to assess calvarial reossification was evaluated by three blinded observers (Fig. 3A). Substantiating our findings by micro-CT reconstructions, a dose-dependent induction of bone healing was observed with SAG. High-dose SAG (1.0 mM) showed significantly higher bone healing scores in comparison to control at both 4 and 8 weeks ($*p < 0.05$; $**p < 0.01$). Intraclass correlation coefficient of 93.9% and 95.1% at each time point showed high interobserver

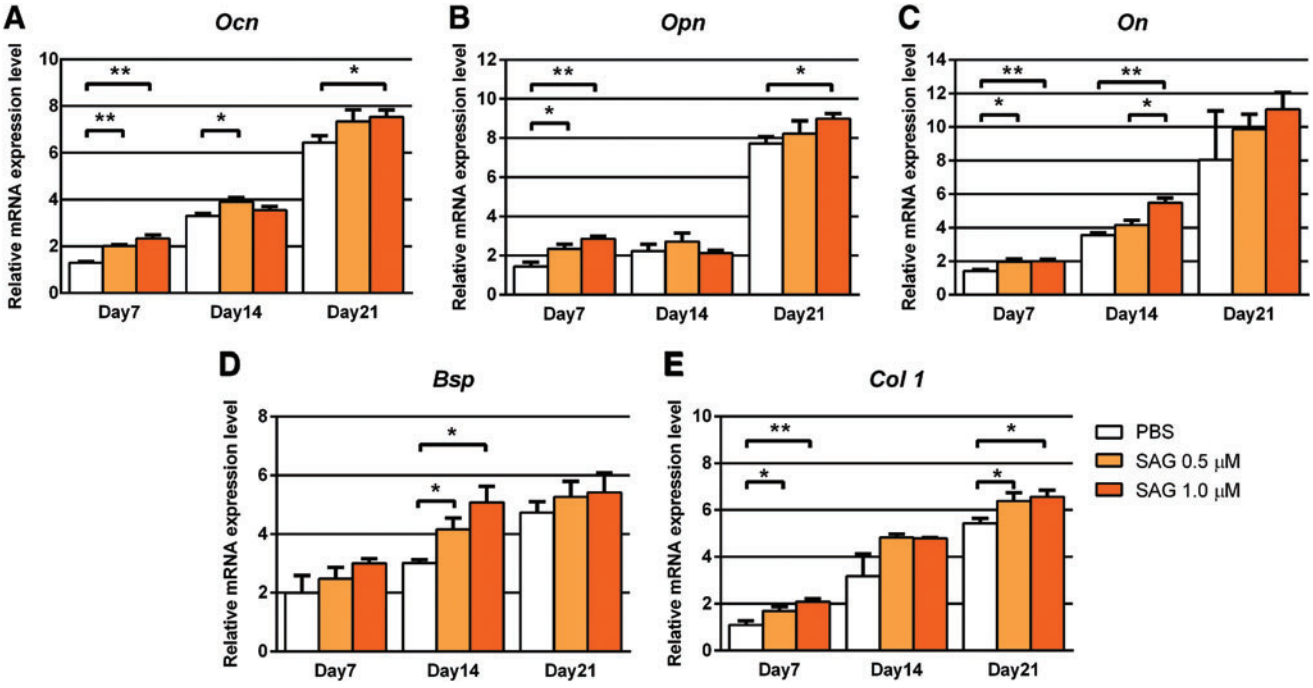

FIG. 1. SAG induces osteogenic differentiation of NMCCs *in vitro*. NMCCs were exposed to the hedgehog agonist SAG (0.5 or 1.0 μM) under osteogenic differentiation conditions for up to 21 days. Gene expression of osteogenic markers at 7, 14, and 21 days, assessed by qRT-PCR. Genes of interest included **(A)** *Ocn*, **(B)** *Opn*, **(C)** *On*, **(D)** *Bsp*, and **(E)** *Col 1*. Experiments performed in triplicate. $*p < 0.05$, $**p < 0.01$ compared to control. SAG, Smoothened agonist; NMCCs, neonatal mouse calvarial cells; qRT-PCR, quantitative real-time polymerase chain reaction; *Ocn (Osteocalcin); Opn (Osteopontin); On (Osteonectin), Bsp (Bone Sialoprotein); Col 1, type I collagen.* Color images available online at www.liebertpub.com/tea

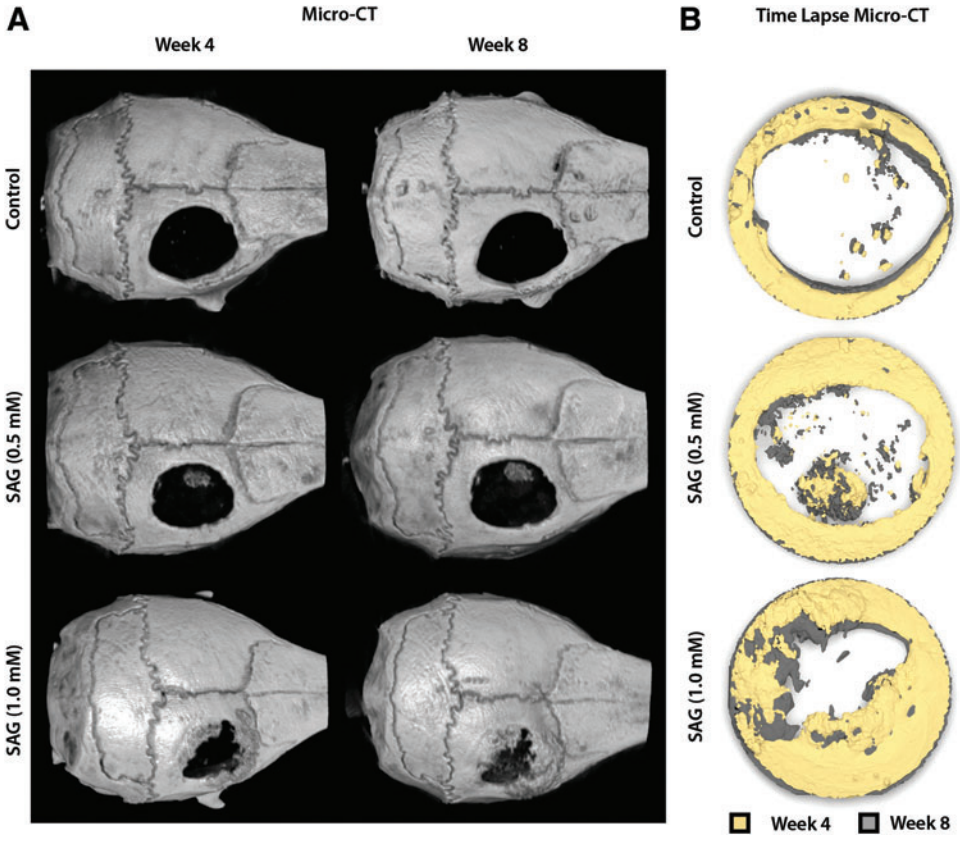

FIG. 2. Representative 3D reconstructed images of calvaria. At 4 and 8 weeks after implantation, the mouse calvaria was imaged using *in vivo* micro-CT. A dose-dependent increase in bone formation within the defect site was observed with SAG treatment. **(A)** Images are whole skull 3D reconstructions and are shown in a top-down perspective. **(B)** Images are time lapse micro-CT reconstructions of the defect site, with color coding of the week 4 and 8 time points. micro-CT, micro-computed tomography; DMSO, dimethylsulfoxide; PLGA, poly(lactic-co-glycolic acid). Color images available online at www.liebertpub.com/tea

agreement in scoring. After generating 2D maximum intensity projections of each group from micro-CT images, BFA was next examined (Fig. 3B). BFA gives an estimate of bony coverage of the underlying brain parenchyma. Results showed a dose-dependent increase in BFA with SAG application, again with significance achieved in the high-dose group (1.0 mM, $^{**}p < 0.01$).

Next, quantitative 3D analyses of micro-CT images were performed of the defect site, again at 4 and 8 weeks postoperative (Fig. 3C, D). Bone volume density (BV/TV) was

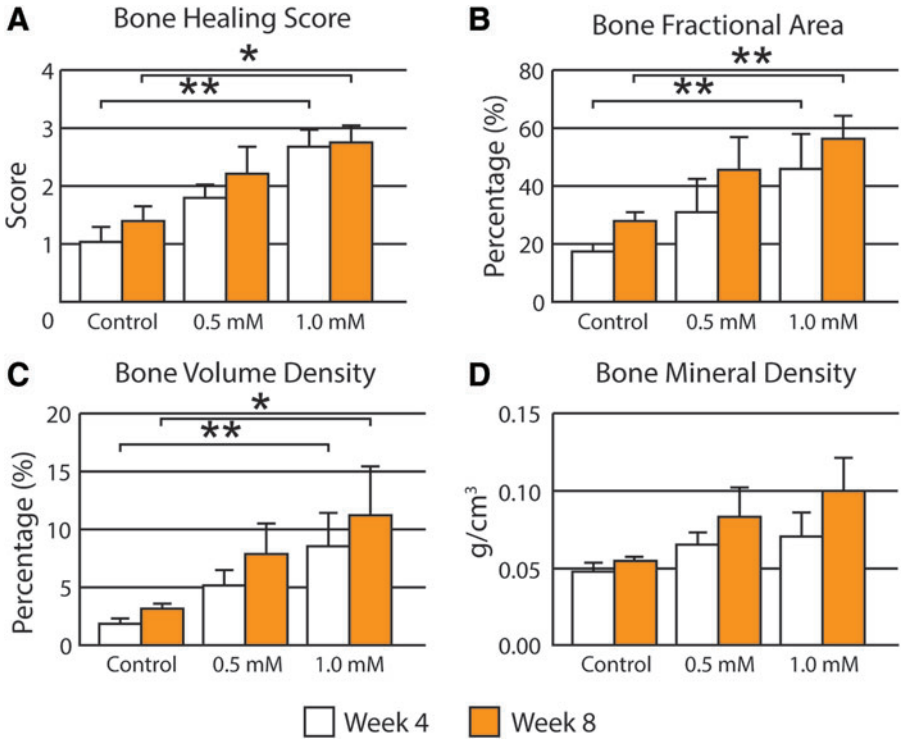

FIG. 3. Micro-CT quantification of bone regeneration in calvarial defects. At 4 and 8 weeks, high-resolution live micro-CT-based quantification and scoring were performed. A score from 0 to 4 was assigned by three independent researchers based on the images attained. For consistent quantification, a 4 mm diameter cylindrical VOI was selected and histomorphometric analyses, including bone volume density and bone mineral density, were performed. **(A)** Bone Healing Score, **(B)** Bone Fractional Area, **(C)** Bone Volume Density, **(D)** Bone Mineral Density. VOI, volume of interest. $^{*}p < 0.05$; $^{**}p < 0.01$. Color images available online at www.liebertpub.com/tea

examined after SAG treatment (Fig. 3C). Confirming prior measurements, high-dose SAG resulted in a significant increase in BV/TV at both 4 and 8 weeks ($*p < 0.05$; $**p < 0.01$). BMD trended toward an increase with SAG application, although this did not achieve statistical significance (Fig. 3D).

Histologic evaluation of bone regeneration. Radiographic findings were next confirmed qualitatively by histologic analysis (Fig. 4). Using H & E and Masson's Trichrome staining, a precipitous cutoff was observed among control-treated defects between the edge of the native parietal bone and adjacent fibrous tissue (black arrowheads indicate the native bone margin). The fibrous tissue of the nonossified defect was intermixed with residual scaffold material (black asterisks) and scattered multinucleated giant cells (red arrowheads). In contrast, SAG treatment resulted in a dose-dependent increase in new woven and lamellar bone formation, which was most prominent at the defect edge, but was also scattered throughout the implantation site. This bone-forming effect was prominent at the high dose of SAG (1.0 mM), while at lower SAG dose, the new bone formation was more subtle. A qualitative increase in neovascularization of the defect site was also seen, especially with high-dose SAG treatment (white arrowheads).

Histomorphometric analysis of the defect site was performed among samples with and without SAG treatment (Fig. 5). Confirming our micro-CT observations, SAG resulted in a dose-dependent increase in Bone Area (B.Ar) and Fractional Bone Area (B.Ar/T.Ar). As mentioned, in routine H & E staining, we observed a qualitative increase in defect vascularization with SAG treatment. To confirm these findings, blood vessel area and number were assessed per high-power field (BV.Ar and BV.N, respectively). SAG induced a significant increase in both parameters of defect vascularity. Overall, SAG treatment alone resulted in significant evidence of calvarial defect healing with combined pro-osteogenic and provasculogenic effects.

Next, immunohistochemical detection of markers of bone healing was performed. These included immunostaining for the osteogenic markers OCN and BSP, as well as VEGF (Fig. 6). BSP and OCN immunohistochemistry decorated the osteoblasts and osteocytes within the new-formed bone with SAG treatment (black arrowheads). Under control treatment conditions, weak or absent staining for OCN and BSP was observed within the fibrous tissue associated with nonhealing defects. VEGF immunostaining was observed within the vasculature associated with new bone formation, as well as less intense staining within osteocytes. As with other markers, weak and minimal VEGF staining was observed under control conditions.

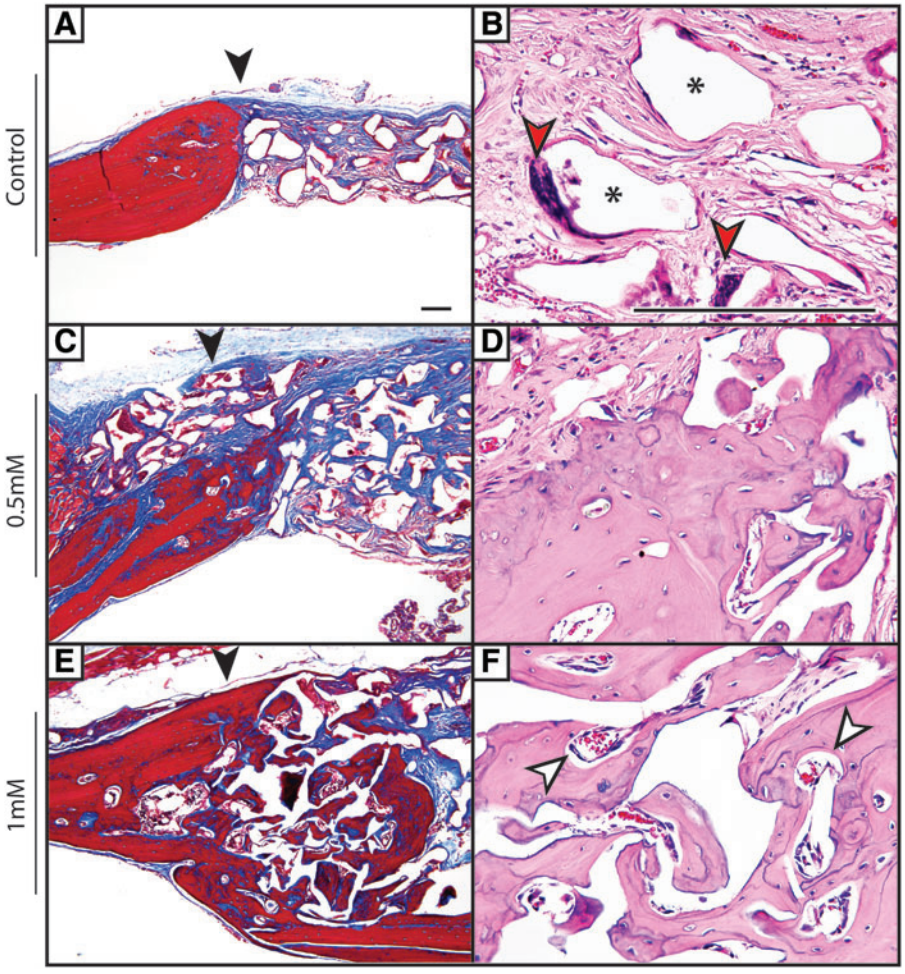

FIG. 4. Histologic analysis of calvarial defect healing. At 8 weeks, postmortem histologic analysis was performed by routine H & E and Masson's Trichrome staining. **(A, B)** Control-treated animals showed a sharp demarcation between the native parietal bone and fibrous tissue (*black arrowhead*) with scattered multinucleated giant cells (*red arrowheads*) and residual scaffold material (*black asterisks*). Scarce new bone formation was observed. **(C, D)** With 0.5 mM SAG, foci of new bone formation was observed, particularly at the defect edge. **(E, F)** With 1.0 mM SAG, significant new lamellar bone was observed, which was predominantly in continuity with the pre-existing parietal bone edge. Significant vascularity of the defect site was also noted in and around the bone interstices (*white arrowheads*). *Black arrowheads* indicate the margin of the native parietal bone. A single representative sample per treatment group is shown. Scale bar = 50 μm. Color images available online at www.liebertpub.com/tea

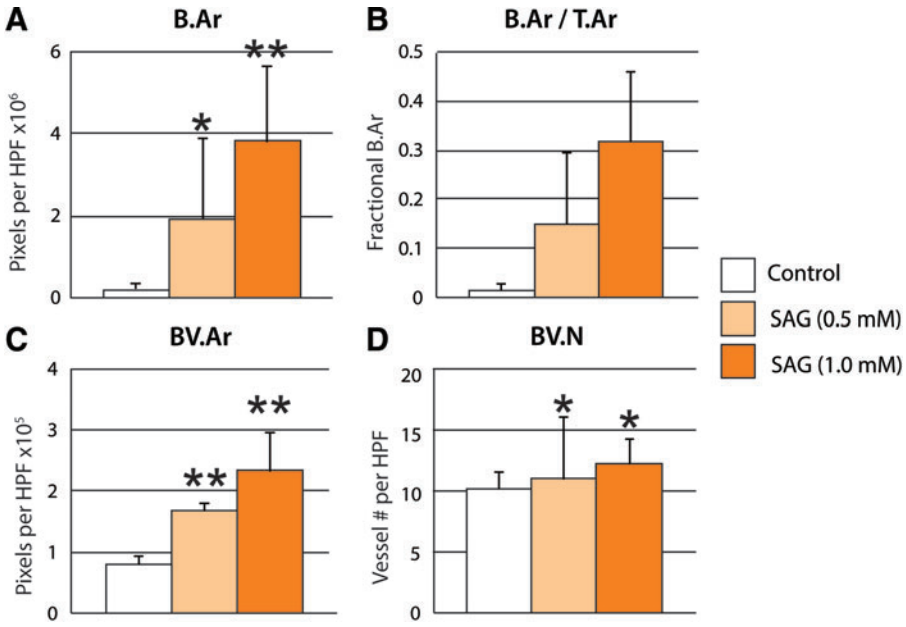

FIG. 5. Histomorphometric analysis of calvarial defect healing. Analyses were performed at the study endpoint (8 weeks). Analyses included **(A)** B.Ar per HPF, **(B)** B.Ar/T.Ar, **(C)** BV.Ar per HPF, and **(D)** BV.N per HPF. Overall, SAG resulted in a dose-dependent increase in endpoints of bone formation and vascularity. $*p < 0.05$; $**p < 0.01$ compared to control. B.Ar, bone area; T.Ar, tissue area; BV.Ar, blood vessel area; BV.N, blood vessel number; HPF, high-power field. Color images available online at www.liebertpub.com/tea

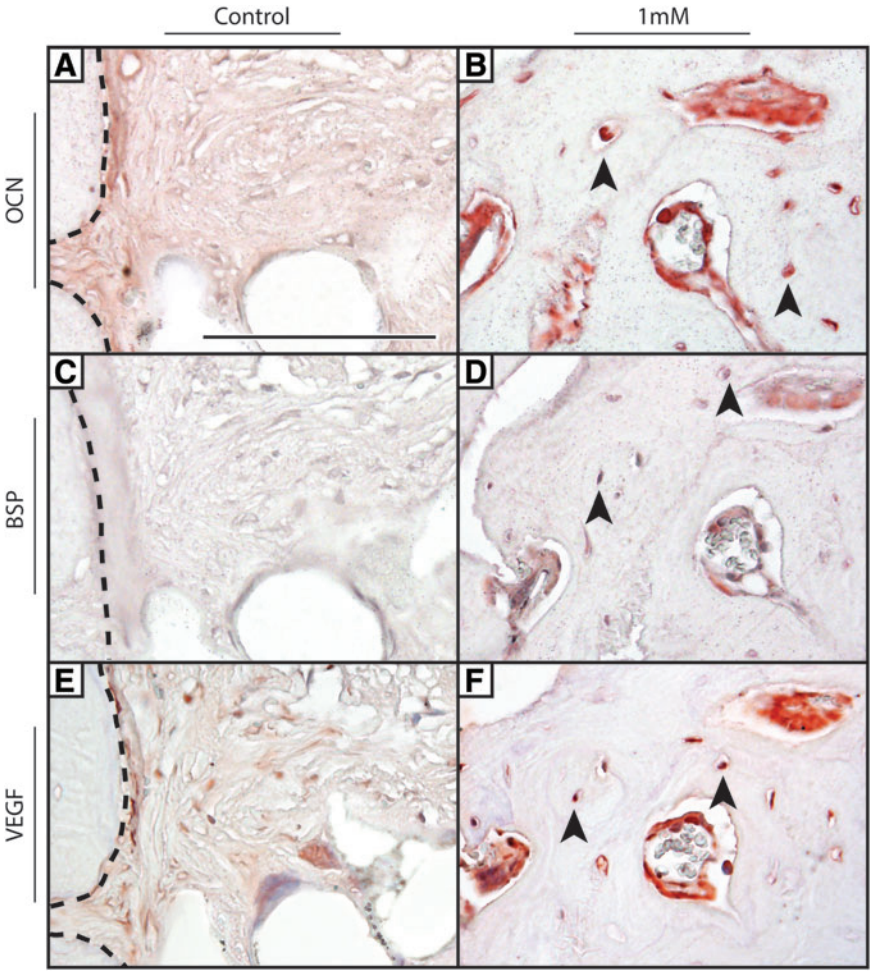

FIG. 6. Immunohistochemical analysis of calvarial defect healing. **(A, B)** OCN, **(C, D)** BSP, and **(E, F)** VEGF expression were interrogated by immunohistochemistry among control- and SAG-treated conditions (1 mM). *Black arrowheads* indicate immunostaining within osteocytes. *Black dashed lines* indicate the native bone defect margin among control samples. A single representative sample per treatment group is shown. Scale bar = 50 μm. OCN, osteocalcin; BSP, bone sialoprotein; VEGF, vascular endothelial growth factor. Color images available online at www.liebertpub.com/tea

Discussion

In this study, we determined the osteogenic potential of the small molecule SAG in a critical-sized mouse calvarial defect model. The results showed that SAG enhanced calvarial osteoblast differentiation *in vitro*, and resulted in a significant and dose-dependent increase in calvarial bone healing *in vivo*. SAG-induced bone healing was also associated with an increased defect neovasculogenesis.

Multiple lines of investigation suggest that modulating Hh signaling may have benefits for postnatal bone healing. For example, upregulated Hh signaling was observed during healing of mouse rib fractures,[37] mouse femoral defects,[17] and rat ulna stress fractures.[38–40] Recently, Ihh was reported to positively regulate not only endochondral ossification but also intramembranous ossification such as the cranial bone.[41] Collectively, ossification is among the notable events regulated by Hh signaling.[42] Priming of adipose-derived stem cells with Shh induces mouse femoral defect healing.[17] Cyclopamine (an Hh antagonist) inhibits mouse calvarial defect healing with or without adipose-derived stem cell application.[43] Recently, Maeda *et al.* examined the application of the small molecule SAG in combination with a helioxanthin derivative (Th) onto tetrapod-shaped calcium phosphate granules for rat unicortical femoral bone defect healing.[44] In this study, the combination of SAG + Th resulted in a significantly increased bone formation in comparison to either alone. Nevertheless, this report is the first known instance of SAG application to a critical- sized bone defect model.

It should be noted that SAG treatment did not result in complete defect reossification in any sample. This may be a result of the large size of our defect model, insufficient or suboptimal dose or duration of SAG, or simply the natural limitations of Hh pathway manipulation in bone healing. The optimal dose for SAG-induced osteogenesis is not yet determined. Our studies used relatively high concentrations (0.5–1.0 mM) based on prior descriptions of SAG in orthopedic application.[44] However, lower doses may be efficacious, especially if the release kinetics for the small molecule are optimized. In addition, previous studies have observed that Hh activation combines with other GDF for improved osteogenesis.[12,17,18] For example, we previously reported that N terminal Shh (Shh-N) combines with BMP2 for induction of osteogenic differentiation in adipose-derived stem cells.[17] Synergy between Shh and BMP-2 has been reported by other investigators.[12] Similarly, Shh-N also exerted combinatorial pro-osteogenic effects with the novel differentiation factor NELL-1.[18] Thus, a combination therapy approach, including the small molecule SAG, may be required for clinically meaningful bone repair. In particular to BMP-2, SAG cotreatment may improve the quality of BMP-2-induced bone repair, which has been reported to be suboptimal across animal models.[45,46]

Importantly, in clinical applications, small-molecule protein-based drugs have substantial advantages over their larger counterparts.[47–53] First, small-molecule medications are usually available for oral administration. Once dissolved in the gastrointestinal tract, the tablet's active material is absorbed through the gut wall into the bloodstream. From this stage, it can be delivered to almost any location in the body given its small molecular size (<1000 Da).[54] Second, small molecules have the capacity for targeting intracellular signaling pathways such as demonstrated with small-molecule biologic therapeutics for inflammation.[55] Third, in general, small molecules do not elicit the unwanted immune responses in the host because of too small a size.[56] Next, unlike protein-based growth factors, the bioactivity of small-molecule compounds is not vitally dependent on higher order structural integrity.[51,57] Last, the cost of manufacturing and risk of contamination between species can be considerably diminished by using small molecules instead of recombinant protein-based growth factors.[51]

In summary, bony nonunion represents a persistent clinical challenge. We observed that the small-molecule SAG induced bone healing in a critical size mouse calvarial defect model. Although SAG did not stimulate complete defect reossification at the dosages examined and in the model system used, its combination with other osteoinductive stimuli represents a promising avenue for future investigation in bone tissue engineering and regenerative medicine.

Acknowledgments

This work was supported by the NIH/NIAMS (grants R01 AR061399, R01 AR066782, K08 AR068316), and the Orthopaedic Research and Education Foundation with funding provided by the Musculoskeletal Transplant Foundation. This research was supported by a grant of the Korea Health Technology R&D Project through the Korea Health Industry Development Institute (KHIDI), funded by the Ministry of Health & Welfare, Republic of Korea (grant number: HI16C1559). The authors would like to thank Spencer Ward for his technical support.

Disclosure Statement

No competing financial interests exist.

References

1. Einhorn, T.A. The cell and molecular biology of fracture healing. Clin Orthop Relat Res **355 Suppl,** S7, 1998.
2. Giannoudis, P.V., Dinopoulos, H., and Tsiridis, E. Bone substitutes: an update. Injury **36 Suppl 3,** S20, 2005.
3. Canady, J.W., Zeitler, D.P., Thompson, S.A., and Nicholas, C.D. Suitability of the iliac crest as a site for harvest of autogenous bone grafts. Cleft Palate Craniofac J **30,** 579, 1993.
4. Kurz, L.T., Garfin, S.R., and Booth, R.E., Jr. Harvesting autogenous iliac bone grafts. A review of complications and techniques. Spine **14,** 1324, 1989.
5. Sandhu, H.S., Grewal, H.S., and Parvataneni, H. Bone grafting for spinal fusion. Orthop Clin N Am **30,** 685, 1999.
6. Sawin, P.D., Traynelis, V.C., and Menezes, A.H. A comparative analysis of fusion rates and donor-site morbidity for autogeneic rib and iliac crest bone grafts in posterior cervical fusions. J Neurosurg **88,** 255, 1998.
7. Shen, J., James, A.W., Zara, J.N., Asatrian, G., Khadarian, K., Zhang, J.B., Ho, S., Kim, H.J., Ting, K., and Soo, C. BMP2-induced inflammation can be suppressed by the osteoinductive growth factor NELL-1. Tissue Eng Part A **19,** 2390, 2013.
8. James, A.W., LaChaud, G., Shen, J., Asatrian, G., Nguyen, V., Zhang, X., Ting, K., and Soo, C. A review of the

clinical side effects of bone morphogenetic protein-2. Tissue Eng Part B Rev **22,** 284, 2016.
9. Hojo, H., Ohba, S., Yano, F., Saito, T., Ikeda, T., Nakajima, K., Komiyama, Y., Nakagata, N., Suzuki, K., Takato, T., Kawaguchi, H., and Chung, U.I. Gli1 protein participates in Hedgehog-mediated specification of osteoblast lineage during endochondral ossification. J Biol Chem **287,** 17860, 2012.
10. Pan, A., Chang, L., Nguyen, A., and James, A.W. A review of hedgehog signaling in cranial bone development. Front Physiol **4,** 61, 2013.
11. Jenkins, D. Hedgehog signalling: emerging evidence for non-canonical pathways. Cell Signal **21,** 1023, 2009.
12. Yuasa, T., Kataoka, H., Kinto, N., Iwamoto, M., Enomoto-Iwamoto, M., Iemura, S., Ueno, N., Shibata, Y., Kurosawa, H., and Yamaguchi, A. Sonic hedgehog is involved in osteoblast differentiation by cooperating with BMP-2. J Cell Physiol **193,** 225, 2002.
13. Kinto, N., Iwamoto, M., Enomoto-Iwamoto, M., Noji, S., Ohuchi, H., Yoshioka, H., Kataoka, H., Wada, Y., Yuhao, G., Takahashi, H.E., Yoshiki, S., and Yamaguchi, A. Fibroblasts expressing Sonic hedgehog induce osteoblast differentiation and ectopic bone formation. FEBS Lett **404,** 319, 1997.
14. Nakamura, T., Aikawa, T., Iwamoto-Enomoto, M., Iwamoto, M., Higuchi, Y., Pacifici, M., Kinto, N., Yamaguchi, A., Noji, S., Kurisu, K., and Matsuya, T. Induction of osteogenic differentiation by hedgehog proteins. Biochem Biophys Res Commun **237,** 465, 1997.
15. Spinella-Jaegle, S., Rawadi, G., Kawai, S., Gallea, S., Faucheu, C., Mollat, P., Courtois, B., Bergaud, B., Ramez, V., Blanchet, A.M., Adelmant, G., Baron, R., and Roman-Roman, S. Sonic hedgehog increases the commitment of pluripotent mesenchymal cells into the osteoblastic lineage and abolishes adipocytic differentiation. J Cell Sci **114,** 2085, 2001.
16. Zhao, M., Qiao, M., Harris, S.E., Chen, D., Oyajobi, B.O., and Mundy, G.R. The zinc finger transcription factor Gli2 mediates bone morphogenetic protein 2 expression in osteoblasts in response to hedgehog signaling. Mol Cell Biol **26,** 6197, 2006.
17. James, A.W., Leucht, P., Levi, B., Carre, A.L., Xu, Y., Helms, J.A., and Longaker, M.T. Sonic Hedgehog influences the balance of osteogenesis and adipogenesis in mouse adipose-derived stromal cells. Tissue Eng Part A **16,** 2605, 2010.
18. James, A.W., Pang, S., Askarinam, A., Corselli, M., Zara, J.N., Goyal, R., Chang, L., Pan, A., Shen, J., Yuan, W., Stoker, D., Zhang, X., Adams, J.S., Ting, K., and Soo, C. Additive effects of sonic hedgehog and Nell-1 signaling in osteogenic versus adipogenic differentiation of human adipose-derived stromal cells. Stem Cells Dev **21,** 2170, 2012.
19. van der Horst, G., Farih-Sips, H., Lowik, C.W., and Karperien, M. Hedgehog stimulates only osteoblastic differentiation of undifferentiated KS483 cells. Bone **33,** 899, 2003.
20. Brunton, S.A., Stibbard, J.H., Rubin, L.L., Guicherit, O.M., Kruse, L.I., Price, S., di Lucrezia, R., MacKinnon, C.H., Avery, A., Park, Y., Buxton, D., and Boyd, E.A. Potent agonists of the Hedgehog signaling pathway. Bioorg Med Chem Lett **19,** 4308, 2009.
21. Chen, J.K., Taipale, J., Young, K.E., Maiti, T., and Beachy, P.A. Small molecule modulation of Smoothened activity. Proc Natl Acad Sci U S A **99,** 14071, 2002.
22. Frank-Kamenetsky, M., Zhang, X.M., Bottega, S., Guicherit, O., Wichterle, H., Dudek, H., Bumcrot, D., Wang, F.Y., Jones, S., Shulok, J., Rubin, L.L., and Porter, J.A. Small-molecule modulators of Hedgehog signaling: identification and characterization of Smoothened agonists and antagonists. J Biol **1,** 10, 2002.
23. Rohatgi, R., Milenkovic, L., and Scott, M.P. Patched1 regulates hedgehog signaling at the primary cilium. Science (New York, NY) **317,** 372, 2007.
24. Hojo, H., Ohba, S., Taniguchi, K., Shirai, M., Yano, F., Saito, T., Ikeda, T., Nakajima, K., Komiyama, Y., Nakagata, N., Suzuki, K., Mishina, Y., Yamada, M., Konno, T., Takato, T., Kawaguchi, H., Kambara, H., and Chung, U.I. Hedgehog-Gli activators direct osteo-chondrogenic function of bone morphogenetic protein toward osteogenesis in the perichondrium. J Biol Chem **288,** 9924, 2013.
25. Kanke, K., Masaki, H., Saito, T., Komiyama, Y., Hojo, H., Nakauchi, H., Lichtler, A.C., Takato, T., Chung, U.I., and Ohba, S. Stepwise differentiation of pluripotent stem cells into osteoblasts using four small molecules under serum-free and feeder-free conditions. Stem Cell Rep **2,** 751, 2014.
26. Zhang, X., Ting, K., Bessette, C.M., Culiat, C.T., Sung, S.J., Lee, H., Chen, F., Shen, J., Wang, J.J., Kuroda, S., and Soo, C. Nell-1, a key functional mediator of Runx2, partially rescues calvarial defects in Runx2(+/-) mice. J Bone Miner Res **26,** 777, 2011.
27. James, A.W., Xu, Y., Wang, R., and Longaker, M.T. Proliferation, osteogenic differentiation, and fgf-2 modulation of posterofrontal/sagittal suture-derived mesenchymal cells in vitro. Plast Reconstr Surg **122,** 53, 2008.
28. James, A.W., Levi, B., Commons, G.W., Glotzbach, J., and Longaker, M.T. Paracrine interaction between adipose-derived stromal cells and cranial suture-derived mesenchymal cells. Plast Reconstr Surg **126,** 806, 2010.
29. James, A.W., Theologis, A.A., Brugmann, S.A., Xu, Y., Carre, A.L., Leucht, P., Hamilton, K., Korach, K.S., and Longaker, M.T. Estrogen/estrogen receptor alpha signaling in mouse posterofrontal cranial suture fusion. PloS One **4,** e7120, 2009.
30. Levi, B., James, A.W., Glotzbach, J.P., Wan, D.C., Commons, G.W., and Longaker, M.T. Depot-specific variation in the osteogenic and adipogenic potential of human adipose-derived stromal cells. Plast Reconstr Surg **126,** 822, 2010.
31. Levi, B., James, A.W., Nelson, E.R., Vistnes, D., Wu, B., Lee, M., Gupta, A., and Longaker, M.T. Human adipose derived stromal cells heal critical size mouse calvarial defects. PLoS One **5,** e11177, 2010.
32. Park, H., Choi, B., Nguyen, J., Fan, J., Shafi, S., Klokkevold, P., and Lee, M. Anionic carbohydrate-containing chitosan scaffolds for bone regeneration. Carbohydr Polym **97,** 587, 2013.
33. Lee, M., Li, W., Siu, R.K., Whang, J., Zhang, X., Soo, C., Ting, K., and Wu, B.M. Biomimetic apatite-coated alginate/chitosan microparticles as osteogenic protein carriers. Biomaterials **30,** 6094, 2009.
34. Umoh, J.U., Sampaio, A.V., Welch, I., Pitelka, V., Goldberg, H.A., Underhill, T.M., and Holdsworth, D.W. In vivo micro-CT analysis of bone remodeling in a rat calvarial defect model. Phys Med Biol **54,** 2147, 2009.
35. Spicer, P.P., Kretlow, J.D., Young, S., Jansen, J.A., Kasper, F.K., and Mikos, A.G. Evaluation of bone regeneration using the rat critical size calvarial defect. Nat Protoc **7,** 1918, 2012.

36. Zhang, X., Peault, B., Chen, W., Li, W., Corselli, M., James, A.W., Lee, M., Siu, R.K., Shen, P., Zheng, Z., Shen, J., Kwak, J., Zara, J.N., Chen, F., Zhang, H., Yin, Z., Wu, B., Ting, K., and Soo, C. The Nell-1 growth factor stimulates bone formation by purified human perivascular cells. Tissue Eng Part A **17,** 2497, 2011.
37. Ito, H., Akiyama, H., Shigeno, C., Iyama, K., Matsuoka, H., and Nakamura, T. Hedgehog signaling molecules in bone marrow cells at the initial stage of fracture repair. Biochem Biophys Res Commun **262,** 443, 1999.
38. Le, A.X., Miclau, T., Hu, D., and Helms, J.A. Molecular aspects of healing in stabilized and non-stabilized fractures. J Orthop Res **19,** 78, 2001.
39. McKenzie, J.A., and Silva, M.J. Comparing histological, vascular and molecular responses associated with woven and lamellar bone formation induced by mechanical loading in the rat ulna. Bone **48,** 250, 2011.
40. Murakami, S., and Noda, M. Expression of Indian hedgehog during fracture healing in adult rat femora. Calcif Tissue Int **66,** 272, 2000.
41. Lenton, K., James, A.W., Manu, A., Brugmann, S.A., Birker, D., Nelson, E.R., Leucht, P., Helms, J.A., and Longaker, M.T. Indian hedgehog positively regulates calvarial ossification and modulates bone morphogenetic protein signaling. Genesis (New York, NY: 2000) **49,** 784, 2011.
42. St-Jacques, B., Hammerschmidt, M., and McMahon, A.P. Indian hedgehog signaling regulates proliferation and differentiation of chondrocytes and is essential for bone formation. Genes Dev **13,** 2072, 1999.
43. Levi, B., James, A.W., Nelson, E.R., Li, S., Peng, M., Commons, G.W., Lee, M., Wu, B., and Longaker, M.T. Human adipose-derived stromal cells stimulate autogenous skeletal repair via paracrine Hedgehog signaling with calvarial osteoblasts. Stem Cells Dev **20,** 243, 2011.
44. Maeda, Y., Hojo, H., Shimohata, N., Choi, S., Yamamoto, K., Takato, T., Chung, U.I., and Ohba, S. Bone healing by sterilizable calcium phosphate tetrapods eluting osteogenic molecules. Biomaterials **34,** 5530, 2013.
45. Zara, J.N., Siu, R.K., Zhang, X., Shen, J., Ngo, R., Lee, M., Li, W., Chiang, M., Chung, J., Kwak, J., Wu, B.M., Ting, K., and Soo, C. High doses of bone morphogenetic protein 2 induce structurally abnormal bone and inflammation in vivo. Tissue Eng Part A **17,** 1389, 2011.
46. Shen, J., James, A.W., Zhang, X., Pang, S., Zara, J.N., Asatrian, G., Chiang, M., Lee, M., Khadarian, K., Nguyen, A., Lee, K.S., Siu, R.K., Tetradis, S., Ting, K., and Soo, C. Novel wnt regulator NEL-like molecule-1 antagonizes adipogenesis and augments osteogenesis induced by bone morphogenetic protein 2. Am J Pathol **186,** 419, 2016.
47. Fu, K., Klibanov, A.M., and Langer, R. Protein stability in controlled-release systems. Nat Biotechnol **18,** 24, 2000.
48. Han, Q.Q., Du, Y., and Yang, P.S. The role of small molecules in bone regeneration. Future Med Chem **5,** 1671, 2013.
49. Hwang, C.J., Vaccaro, A.R., Lawrence, J.P., Hong, J., Schellekens, H., Alaoui-Ismaili, M.H., and Falb, D. Immunogenicity of bone morphogenetic proteins. J Neurosurg Spine **10,** 443, 2009.
50. Kessler, M., Goldsmith, D., and Schellekens, H. Immunogenicity of biopharmaceuticals. Nephrol Dial Transplant **21 Suppl 5,** v9, 2006.
51. Lo, K.W., Ashe, K.M., Kan, H.M., and Laurencin, C.T. The role of small molecules in musculoskeletal regeneration. Regen Med **7,** 535, 2012.
52. Lo, K.W., Jiang, T., Gagnon, K.A., Nelson, C., and Laurencin, C.T. Small-molecule based musculoskeletal regenerative engineering. Trends Biotechnol **32,** 74, 2014.
53. Segar, C.E., Ogle, M.E., and Botchwey, E.A. Regulation of angiogenesis and bone regeneration with natural and synthetic small molecules. Curr Pharm Design **19,** 3403, 2013.
54. Kidane, A., and Bhatt, P.P. Recent advances in small molecule drug delivery. Curr Opin Chem Biol **9,** 347, 2005.
55. Mocsai, A., Kovacs, L., and Gergely, P. What is the future of targeted therapy in rheumatology: biologics or small molecules? BMC Med **12,** 43, 2014.
56. Laurencin, C.T., Ashe, K.M., Henry, N., Kan, H.M., and Lo, K.W. Delivery of small molecules for bone regenerative engineering: preclinical studies and potential clinical applications. Drug Discov Today **19,** 794, 2014.
57. Wieghaus, K.A., Capitosti, S.M., Anderson, C.R., Price, R.J., Blackman, B.R., Brown, M.L., and Botchwey, E.A. Small molecule inducers of angiogenesis for tissue engineering. Tissue Eng **12,** 1903, 2006.

Address correspondence to:
Aaron W. James, MD, PhD
Department of Pathology
Johns Hopkins University
720 Rutland Avenue, Room 524A
Baltimore, Maryland 21205

E-mail: awjames@jhmi.edu

Received: April 27, 2016
Accepted: September 13, 2016
Online Publication Date: October 18, 2016